STM studies on the island dynamics on Au(100) electrodes in sulfuric acid

2002 J. Phys.: Condens. Matter 14 4211

(http://iopscience.iop.org/0953-8984/14/16/312)

INSTITUTE OF PHYSICS PUBLISHING JOURNAL OF PHYSICS: CONDENSED MATTER

J. Phys.: Condens. Matter **14** (2002) 4211–4225 PII: S0953-8984(02)29070-0

STM studies on the island dynamics on Au(100) electrodes in sulfuric acid

Sabine Dieluweit and Margret Giesen[1,2]

Institut für Schichten und Grenzflächen, ISG 3, Forschungszentrum Jülich, D 52425 Jülich, Germany

E-mail: m.giesen@fz-juelich.de

Received 25 September 2001
Published 11 April 2002
Online at stacks.iop.org/JPhysCM/14/4211

Abstract

We have studied the dynamics of monolayer Au islands on a Au(100) electrode in sulfuric acid using electrochemical scanning tunnelling microscopy. We present quantitative studies of the equilibrium shape of Au islands on Au(100) electrodes and of the thermal fluctuations around the equilibrium shape. As was recently demonstrated for islands on metal surfaces under ultra-high vacuum (UHV), step and kink energies may be determined. Furthermore, we present data on the decay of Au islands on Au(100) electrodes due to Ostwald ripening and due to the reformation of the potential-induced reconstruction on the gold electrode. In both cases we observe that different dominant mass transport processes control the island decay. In the case of island decay during potential-induced reformation of the reconstruction, we find furthermore evidence for rapid island decay processes as were recently reported for metal surfaces in UHV studies.

1. Introduction

In recent years much effort has been spent to study and understand the structure of electrode surfaces in the liquid environment as well as the kinetics and dynamics of defects at the solid/liquid interface. The detailed understanding of defects on metal electrodes is of particular importance for the understanding of metal deposition from the liquid onto the solid electrode [1–16], for the understanding of the coarsening on electrode surfaces during 'electrochemical annealing' [17–20] as well as for corrosion processes [21]. Although it is well known that defects play a significant role in electrode reactions, the available information and data is generally merely qualitative. For surfaces under ultra-high vacuum (UHV) conditions, however, the dynamics of defects has been studied quantitatively for more than a decade now

[1] Author to whom any correspondence should be addressed.
[2] http://www.fz-juelich.de/isg/isg3/Giesen/ag-giesen1.htm.

(for an overview see e.g. [22, 23]). To overcome the information gap for metal electrodes in an electrolyte, several years ago we (among others [24–30]) started to apply theoretical methods developed for studies of defects on metal surfaces in UHV to surfaces in contact with a liquid [23,31–36]. For example, we were able to determine diffusion barriers and kink energies on metal electrodes by studying equilibrium fluctuations of monatomic steps [23,31–33,35]. It must be emphasized that the used theoretical concepts merely require that the thermodynamical equilibrium of the system is determined by the minimum in the Gibbs free energy. The Gibbs free energy itself is directly related to interfacial energies (such as surface energies and step energies) and to formation energies (such as kink energies). Compared to UHV, these quantities may of course be altered by the presence of the liquid, the change of the energetic parameters, however, will merely result in characteristic modifications of the equilibrium state of the solid/liquid interface or of the pathway the system takes to reach equilibrium. It is precisely these modifications in which we are interested in. In the present work we demonstrate that one may determine kink and step free energies at the solid/liquid interface by the analysis of island equilibrium shapes [37] and island shape fluctuations [38–40] as was recently reported for metal islands in UHV.

Further information on surface diffusion on electrodes in contact with a liquid may be gained by studies of the ripening of island structures at the solid/liquid interface. Island decay studies under UHV conditions are frequently reported (for an overview see e.g. [23]). Similar studies on metal electrodes in electrolyte are still rare [20,24,27–30,41,42]. With this work, we would like to contribute to this promising field with a study which focuses on the island coarsening on Au(100) electrodes. We have performed two different measurements: the first one is related to the normal Ostwald ripening of monolayer islands via intralayer mass transport at high potentials. The second considers the island decay after a potential step to negative electrode potentials where the surface reconstruction of the Au(100) surface is re-established and the island decay is dominated by interlayer mass transport.

The paper is organized as follows: in section 2, we describe the experimental set-up and briefly review the theoretical methods we used to analyse our data. The experimental results are presented in section 3 followed by a discussion in section 4. The results will be summarized in section 5.

2. Experimental and theoretical methods

2.1. Experimental set-up

The measurements were performed with the electrochemical version of the Topometrix TMX 2010 discoverer scanning tunnelling microscope (STM). This instrument was modified to enable temperature variable STM recording with high thermal drift stability and is described in detail elsewhere [34, 35]. In the studies reported here, however, all experimental results were obtained at 297 K. The tip and the sample potential are independently controlled via a bipotentiostat.

The Au(100) electrodes were cut by spark erosion from a single crystal rod, oriented by diffractometry and polished to the desired orientation to within 0.1°, which is the accuracy of high-quality single crystals. The accuracy is naturally limited by the mosaic structure of the crystal. Prior to experiment, the Au(100) electrode was heated in a hydrogen atmosphere and then flame annealed for 5 min to about 900°C. The temperature was visually controlled by the colour of the annealed crystal. After thoroughly rinsing the cell with Milli-Q water (18.2 MΩ cm^{-1}), the crystal was mounted to the electrochemical STM cell which was connected to the bipotentiostat. The crystal surface was then brought in contact with the

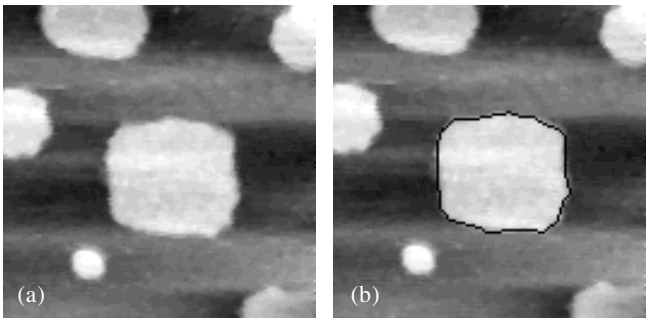

Figure 1. STM image of a Au island on Au(100) at +400 mV versus SCE (56×56 nm^2) (*a*) before and (*b*) after running the computer code to find the island perimeter. The black line in (*b*) is the determined perimeter which is used for further analysis.

electrolyte under potential control. This was visually checked for at the beginning of each STM experiment by the presence of the well-ordered quasi-hexagonal reconstruction of the clean Au(100) surface [41, 43, 44]. The mean terrace width of the crystal was of the order of several 100 nm. As an electrolyte, we used suprapure H_2SO_4 (Merck) and Milli-Q water (Millipore, 18.2 MΩ cm^{-1}). In all experiments, the concentration of the electrolyte was 50 mM.

The tunnelling tips used in the experiments were etched from polycrystalline tungsten wires and coated with polyethylene to avoid Faraday currents at the foremost part of the tip. We used a tunnelling current of 2 nA and the tip bias was held constant at -0.07 V versus SCE to avoid oxidation of the tungsten tip. That means the tunnelling resistance varied between 0.19 and 0.39 GΩ for electrode potentials between +300 and +700 mV versus SCE. The typical time per image was 40–60 s and the STM images were recorded with a 400×400 pixel resolution in the constant current mode. High-purity, flame-annealed Pt wires (Goodfellow, 99.999%) served as counter and quasi-reference electrodes. In the following, the electrode potentials of the metal sample are, however, given with respect to the saturated calomel electrode (SCE).

The island shapes of individual islands in the STM images are determined by a special computer code which searches for the maximum slope in the grey scale in an STM image. Starting at a distinct point in the centre of an island, the program finds the radius of an island for a given polar angle. The accuracy of the overall shape is given by the step width between individual polar angles which can be chosen to a minimum value of 1° (in other words by the number of base points, at maximum 360), by the pixel noise and by the noise in the STM image. In the experiments reported here, the island shapes were determined using 200 base points (i.e. 200 number pairs consisting of the island radius and the corresponding polar angle). Figure 1 shows (*a*) an STM image of a Au island on Au(100) before and (*b*) after the island has been found and marked (black line) by the computer code. For the analysis we carefully checked the obtained island perimeters by visual inspection and made sure that the island area deviations introduced by the computer code was at maximum 1% (i.e. the error in the mean island radius is less than 0.5%).

2.2. Theoretical methods to analyse equilibrium island shapes

Determination of kink and step energies by studies of the local curvature of island shapes. In [37] we showed that the local curvature of the equilibrium shape $\theta = 0$ of an island is related to the step free energy $\gamma(\theta)$ via

$$y\frac{\partial^2 y}{\partial x^2}\tilde{\gamma}(\theta=0)=\gamma(\theta=0). \tag{1}$$

Here, $\tilde{\gamma}(\theta)$ is the step edge stiffness [45] of the island perimeter at polar angle θ, which is given by

$$\tilde{\gamma}=\gamma+\frac{\partial^2\gamma}{\partial\theta^2}. \tag{2}$$

The angle θ is chosen such that $\theta=0$ corresponds to the $\langle 110\rangle$-orientation of a step segment in the island perimeter. In (1) and in the following Cartesian coordinates x, y are chosen such that $x=0$ for $\theta=0$. The step edge stiffness may be expressed by the diffusivity b^2, $\tilde{\gamma}=\frac{k_BT}{b^2}a_{\parallel}$. In the limit of low temperatures (i.e. for kinks of monatomic length), the diffusivity may be written in terms of the kink concentration such that $b^2\approx 2\exp\left(-\frac{\varepsilon}{k_BT}\right)a_{\perp}^2$ (with ε the kink energy and $a_{\parallel}$, $a_{\perp}$ the distances between atomic rows along and perpendicular to $\langle 110\rangle$; $a_{\parallel}=a_{\perp}$ for (100) surfaces) [45]. Then, one eventually has [37]

$$y\frac{\partial^2 y}{\partial x^2}k_BT\approx 2\gamma\, a_{\parallel}\exp\left(-\frac{\varepsilon}{k_BT}\right) \tag{3}$$

where we used $a_{\perp}=a_{\parallel}$ for (100) surfaces.

From (3) it becomes obvious that temperature variable data on the local curvature and the island radius at $\langle 110\rangle$-oriented island segments are sufficient to determine the kink and the step energy. In an Arrhenius-plot of the left-hand side of (3) the kink energy is given by the slope and the step energy by the intersection. If temperature-variable data is not available either the kink energy or the step energy must be independently determined from a different measurement. The kink energy may be measured by analysing the spatial equilibrium fluctuations of monatomic steps (for recent reviews see [22, 23]). Data on the step energy may be obtained from the analysis of the equilibrium fluctuations of the island shape which is discussed in the next paragraph.

Determination of step energies by island shape fluctuation studies. The relation between the magnitude of island shape fluctuations and the mean step free energy is derived using a capillary mode analysis of Khare and Einstein [38] which was applied to island fluctuation studies by Schlößer *et al* [39] and recently also by Steimer *et al* [40]. In equilibrium, the island shape represents a minimum in the free energy of the island. Due to the island edge fluctuations, the time average of the total free energy is larger by a distinct amount. The fluctuation function $\langle G(\bar{r})\rangle_t$ determines the time average of the deviations of the island shape from its equilibrium shape and is given by

$$\langle G(\bar{r})\rangle_t=\frac{3k_B\bar{r}\,T}{4\pi\bar{\gamma}}. \tag{4}$$

Here, $\bar{r}$ is the mean radius of a fluctuating island and $\bar{\gamma}$ is the mean step free energy along the island perimeter. Details of the derivation and the validity of (4) in specific limits are given in [40].

2.3. Theory of island decay

So far we have considered the islands on the surface as to be in quasi-equilibrium, i.e. the islands assume their equilibrium shape save for thermal fluctuations around the minimum free energy shape (for a given area). The existence of islands on the surface, however, indicates that the surface structure itself is not in equilibrium. Islands on the surface enhance locally the chemical potential of the surface. The spatial gradient in the chemical potential is the

driving force for a coarsening of the surface structure by means of island coalescence and/or island decay. The chemical potential $\mu(R)$ of an island with radius R is given by the famous Gibbs–Thomson relation[3]

$$\mu(R) = \Omega\frac{\gamma}{R} \tag{5}$$

where γ is the step free energy as in (2) and $\Omega = a_{\parallel}a_{\perp}(=a_{\parallel}^2$ for (100) surfaces) is the atomic unit factor. Equation (5) is valid for square or hexagonal-shaped islands if R is defined as $R = y(x = 0)$. In the classical theory of Ostwald ripening [46,47] the difference in chemical potential leads to a mass transport current directed from small to large islands [48,49]. The time evolution of the island areas is determined by the balance in the time-limiting mass transport processes. Two limiting cases may be distinguished (for details see e.g. [23]): in the first case, the time-limiting transport is the diffusion of mass species on the terraces. Then, the island decay is denoted as *diffusion limited* and the change of the island area $A(t)$ in time is given by

$$\frac{\mathrm{d}A(t)}{\mathrm{d}t} \approx -\frac{2\pi\nu_0\Omega}{\ln|R/r|}\exp[-(E_{ad} + E_{diff})/k_BT]\frac{\eta\gamma\Omega}{k_BT}(1/r - 1/R). \tag{6}$$

Here, R and r denote the radii of the large and the small island, respectively. ν_0 and E_{diff} are the pre-exponential factor and the activation barrier for terrace diffusion. E_{ad} denotes the creation energy for terrace adatoms from kinks in the island edge. Equation (6) assumes the islands to be circular such that the area is given by $A = \pi r^2$, respectively πR^2. In this case, the deviation of hexagonal and square islands from a circular shape is considered by introducing a shape factor η [50]. By integrating (6), one finds for the time dependence of the island area in the *diffusion limited* case

$$A(t) \propto (t_0 - t)^{2/3}. \tag{7}$$

In the second case, the time-limiting transport process is the detachment of atoms from kinks at the island edge. Then, the island decay is denoted as *detachment limited* and the change of the island area $A(t)$ in time is given by

$$\frac{\mathrm{d}A(t)}{\mathrm{d}t} \approx -2\pi\nu_0\Omega s\exp[-(E_{ad} + E_{diff})/k_BT]\frac{\eta\gamma\Omega}{ak_BT}(1 - r/R). \tag{8}$$

In (8), the sticking rate at the island edge is denoted as 's' and 'a' is an atomic unit factor determined by the nearest neighbour distance of equivalent hopping sites on the terrace. By integrating (8), one finds for the time dependence of the island area in the *detachment limited* case

$$A(t) \propto (t_0 - t). \tag{9}$$

The equations derived above are strictly valid only under the assumption that the small (adatom) island is located within the centre of a large (vacancy) island. Furthermore, the step free energy γ is assumed to be small, i.e. $\eta\gamma\Omega/k_BT \ll 1$. Last but not least, the ratio of the radii of the small and the large island is considered to be approximately time independent, i.e. $\ln|r/R|$ is considered as constant. For details we refer to [23,50].

3. Experimental results

3.1. Equilibrium shape of Au islands on Au(100)

It is well known that the Au(100) electrode in sulfuric acid undergoes a phase transition: at low electrode potentials the surface reveals a quasi-hexagonal (hex)-reconstruction with

[3] Without restriction of generality, we neglect in equation (5) the constant contribution of the chemical potential μ_∞ far away from the island.

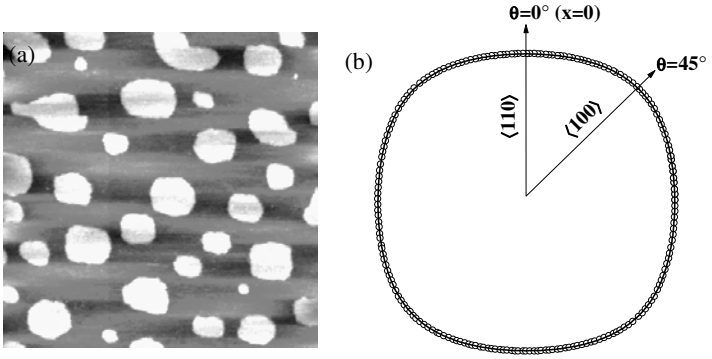

Figure 2. (*a*) STM image of Au islands on Au(100) at +400 mV versus SCE (surface area 171 × 171 nm^2). (*b*) Equilibrium shape determined from more than 500 individual, fluctuating islands.

a 24% higher surface density than the (1 × 1) unreconstructed (100) surface [51–53]. At the potential of zero charge (pzc) at about +280 mV versus SCE[4], sulfate anions from the electrolyte are specifically adsorbed to the surface and the reconstruction is lifted. Due to the lifting of the reconstruction adatoms are added to the surface layer and monatomic high islands nucleate. Figure 2(*a*) shows an STM image of the Au(100) electrode at room temperature and +400 mV versus SCE after island formation. The surface area is 171 × 171 nm^2. The islands in an STM image (which represents only a snap shot of the surface) are about quadratic in shape, the perimeter of an individual island in an STM image, however, may considerably deviate from the (100) surface symmetry: this is due to island shape fluctuations arising from atomic motion at the island perimeter as was previously reported by Dakkouri [20] and will be discussed in detail below. As displayed also in figure 2(*a*), some shapes are caused by coalescence events between neighbouring islands. In later frames of a whole STM series these coalesced islands will recover a quadratic shape again. From images similar to that shown in figure 2(*a*) and from more than 500 individual islands, we determined the equilibrium shape of the Au islands which is plotted in figure 2(*b*)[5]. The circles represent the experimental data and the solid line is a fit to the equilibrium shape using the Ising model [37]. The Ising parameter obtained from such a fit is comparable though not identical to the kink energy if the step free energy per atom is of the same order as the kink energy [23, 32]. For quasi-hexagonal islands on (111) surfaces of fcc metals this is generally the case, while for islands on (100) surfaces γ may significantly deviate from ε [37]. Therefore, the analysis of the Ising parameter is not considered in this work. Detailed studies of the Ising parameter for the Au(100) electrode are left to future work.

It is due to the large shape fluctuations that a large data set of individual island shapes are necessary to determine the equilibrium shape. In the next section, we use the equilibrium shape as shown in figure 2(*b*) to determine the curvature of the ⟨110⟩-oriented segments of the island perimeter.

[4] This value is the pzc for the defect-free surface. Since the local work function at a step may deviate from the surface work function [54], the pzc may be expected to be slightly shifted in the presence of islands and steps [55].

[5] We note that the equilibrium shape is determined from the average over individual shapes as measured in the STM images. These individual shapes may significantly deviate from the equilibrium shape due to the island shape fluctuations as discussed later. As has been shown in [39,40] the time average over the island shape fluctuations yields the equilibrium shape as long as the fluctuations are statistically independent.

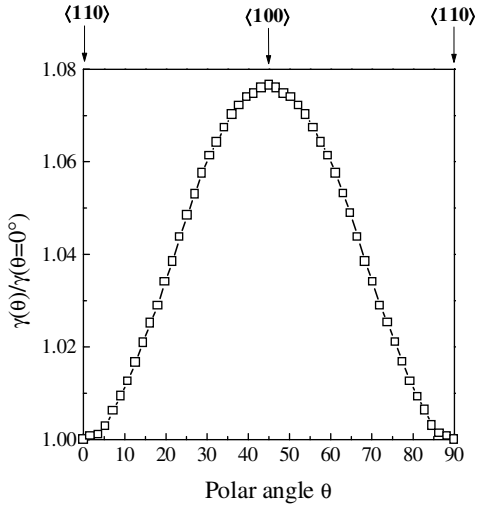

Figure 3. Normalized angle dependence of the step free energy $\gamma(\theta)$ for Au islands on Au(100) in H_2SO_4 at +400 mV versus SCE at 297 K determined from the equilibrium shape as displayed in figure 2(*b*).

From the equilibrium shape one may also determine the so-called γ-plot which denotes the normalized angle dependence of the step free energy $\gamma(\theta)$. For the high-symmetry directions $\langle 110\rangle$ and $\langle 100\rangle$ (corresponding to $\theta = 0^\circ$ and 45°, respectively) the ratio of the island radii $r(\theta = 45^\circ)/r(\theta = 0^\circ)$ is equal to the ratio of the step free energies $\gamma_{\langle 100\rangle}/\gamma_{\langle 110\rangle}$. In figure 3, $\gamma(\theta)/\gamma(\theta = 0^\circ)$ is given for Au islands on the Au(100) electrode in 50 mM H_2SO_4 at +400 mV versus SCE at 297 K. The ratio between 100% kinked steps along $\langle 100\rangle$ and steps along the dense $\langle 110\rangle$-direction, $\gamma_{\langle 100\rangle}/\gamma_{\langle 110\rangle}$, is found to be $\gamma_{\langle 100\rangle}/\gamma_{\langle 110\rangle} = 1.077 \pm 0.001$.

3.2. Measurement of the step curvature around $\langle 110\rangle$*-segments of Au islands on Au(100)*

The curvature of the $\langle 110\rangle$ step segments of the island equilibrium shape is measured by converting first the polar coordinates into the corresponding Cartesian coordinates. For further analysis merely the part of the equilibrium shape is considered, which is adjacent to the centre point of the $\langle 110\rangle$ segments. In other words, if the centre of the $\langle 110\rangle$ segment is denoted as $\theta = 0$, only data points within an angle range $\pm\Delta\theta$ are taken into account which are still far from the rounded corners at $\theta = 45^\circ$. The accuracy of the measurement of the curvature of the $\langle 110\rangle$ step segments is limited by two factors: first, the larger the value of $\Delta\theta$, the larger is the error introduced by the curvature of the rounded corners at $\theta = 45^\circ$. Second, if $\Delta\theta$ is too small, the number of data points available to determine the curvature becomes too small and the statistical error may be large. One way to handle this problem is to analyse the curvature for various $\Delta\theta$. We have checked the results for angle deviations between $\pm 6^\circ$ and 18°. The obtained curvature values do not change if the data set is large and the noise in the data for the equilibrium shape is small. For smaller data sets, the value of the curvature systematically decreases with decreasing angle variation, however, the error bars for the obtained value of $y \cdot y''$ become large because of the small number of base points for the Taylor expansion fit. Here, we discuss merely the results for $y \cdot y''$ obtained for one distinct angle variation. The most reliable one appeared to be the data analysed with $\Delta\theta = \pm 15^\circ$. The data points around $\theta = 0$ are fitted by a Taylor expansion to second order. The curvature is then given by twice

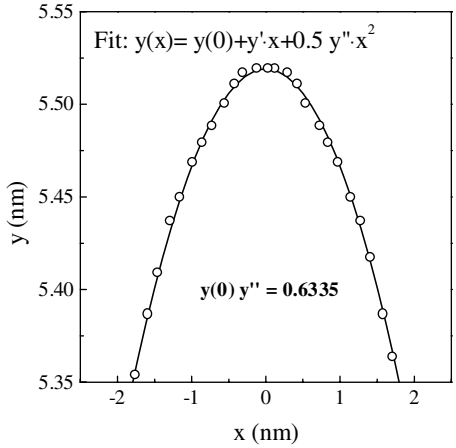

Figure 4. Determination of the local curvature at $y(0)$ of a $\langle 110 \rangle$-oriented perimeter segment using the equilibrium shape as shown in figure 2(*b*). See text for further discussion.

the pre-factor of the second-order term in the expansion. Figure 4 shows the perimeter of the equilibrium shape for the $\langle 110 \rangle$-segment around $x = 0$ and for a variation $\pm\Delta\theta = \pm 15^\circ$ around the polar angle $\theta = 0$. From a fit to the data with a power expansion to second order we obtain

$$y(0) \left.\frac{\partial^2 y}{\partial x^2}\right|_{x=0} = 0.6335. \tag{10}$$

Here, $y(0)$ denotes the local radius at the centre of the $\langle 110 \rangle$ step segment and $\left.\frac{\partial^2 y}{\partial x^2}\right|_{x=0}$ is the curvature at $y(0)$. In paragraph 4, the result of (10) will be used to measure the kink energy according to (3).

3.3. Analysis of the shape fluctuations of Au islands on Au(100)

Figure 5 shows two individual island perimeters of a fluctuating island at $t = 17$ (circles) and 20 min (triangles) of the STM series. For comparison, the equilibrium shape (as already shown in figure 2) is plotted as a solid line. Figure 6 displays the time average of the deviation function $\langle G(\bar{r}) \rangle_t$ as defined in (4) versus the product of the island radius and the temperature. Since the islands used for the analysis undergo coarsening via Ostwald ripening, the island area changes during STM recording. Therefore we have divided the analysed islands in sub-sets of islands of about equal area where we allowed area deviations of 10% at maximum. These sub-sets were analysed with respect to the shape fluctuations separately. Each data point in figure 6 corresponds to one of these sub-sets. From a linear fit to the data in figure 6 we find a slope of

$$(1.0 \pm 0.1) \times 10^{-4} \text{ nm K}^{-1} \tag{11}$$

which corresponds according to (4) to

$$\bar{\gamma}\, a_\parallel = 59 \pm 6 \text{ meV}. \tag{12}$$

Using this result and (10) in (3), we find finally for the kink energy

$$\varepsilon = 51 \pm 3 \text{ meV} \tag{13}$$

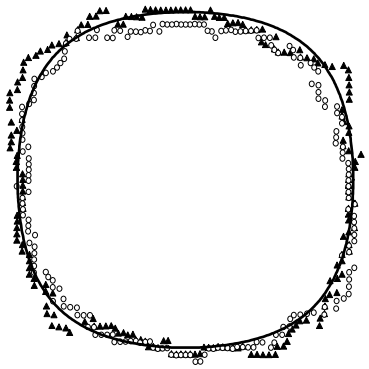

Figure 5. Two individual island perimeters taken from the STM images at $t = 17$ (circles) and 20 min (triangles) of a STM series compared to the equilibrium shape (solid curve) which is determined from averaging over more than 500 individual island perimeters.

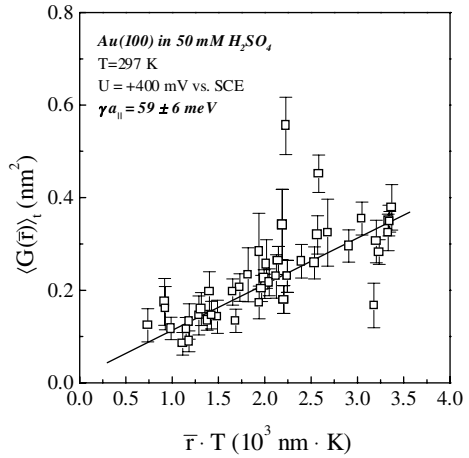

Figure 6. Plot of $\langle G(\bar{r})\rangle_t$ for various island radii $\bar{r}$ according to (4).

3.4. Island decay on the Au(100) electrode in sulfuric acid

We have investigated the decay of Au islands on Au(100) in 50 mM H_2SO_4 for two different cases: first, we have studied the decay of islands due to normal analysed ripening at +500 mV versus SCE where the surface is unreconstructed. Some island decay curves are shown in figure 7(*a*). The measured curves are typical for a *diffusion limited* decay mechanism [50, 56, 57], and the decay of the size of small islands (islands 1–4) is described by a potential law similar to (7). Large islands (islands 5–6), on the other hand, serve as sinks for the atoms detached from small islands and thence hardly decay or even grow in size. The interaction between neighbouring islands is a strong indication for diffusion limited island decay [50, 57].

In the second case, islands were created at +400 mV versus SCE. Subsequently, the potential was stepped back to −150 mV versus SCE where the (hex) surface reconstruction is re-established. Atoms are incorporated into the surface layer to form the reconstruction lines. These atoms stem from steps on the surfaces as well as from monolayer islands. As a consequence, the islands shrink in size. Figure 7(*b*) shows several decay curves measured in

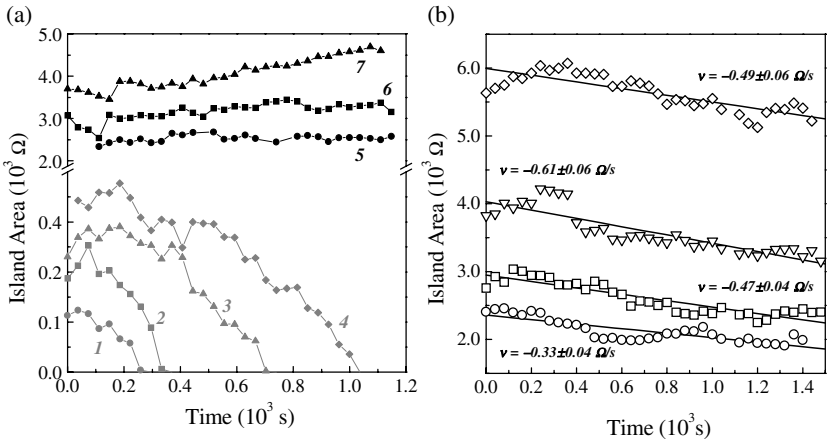

Figure 7. Au island decay curves on Au(100) in 50 mM H_2SO_4 at (*a*) +500 mV versus SCE and (*b*) −150 mV versus SCE (after island creation at +400 mV). In case (*a*), the islands undergo normal Ostwald ripening via diffusion limited decay whereas in case (*b*), where the island decay is due to the re-formation of the (hex) reconstruction, the decay is detachment limited. Note the axis break and the different scales in (*a*).

such an experiment. The decay curves are obviously different from those in figure 7(*a*) and are best fitted by a linear curve according to (9). Hence, the island decay is *detachment limited*. The measured decay rates lie between −0.33 and −0.61 atom s^{-1}.

From inspecting STM movies[6] of the island decay we found evidence for rapid interlayer mass transport as has been recently reported for Cu(111) [58, 59] and Ag(111) [60] in UHV. Frequently, when a reconstruction line evolves across the surface and approaches a Au island, the atoms in the island seem to 'dive' into the terrace below and the reconstruction line becomes longer. Figure 8 shows a decay curve of an island during such an event. Initially, the island decays linearly with a rate of about −0.28 atom s^{-1}. When the reconstruction lines comes close to the island (arrow 1), the decay rate increases to −3.92 atom s^{-1}. Eventually, the island separates from the reconstruction line again (arrow 2). Then, the fast decay process stops and the decay rate is −0.23 atom s^{-1}.

4. Discussion

We have separated the discussion in two sections: first, we discuss the results on the step and kink energy from the island shape and fluctuations studies. In the second section, we examine the data on the island decay measurements.

4.1. Step and kink energy on Au(100) in 50 mM H_2SO_4

To the best of our knowledge, no theoretical or experimental data (other than those presented here) on step and kink energies are available. One may therefore compare the results for the step and the kink energy merely with UHV data. In doing so, however, one should keep in mind that the Au(100) surface in sulfuric acid at high electrode potentials may be considerably different from Au(100) in UHV due to the presence of the liquid and, in particular, due to the specific adsorption of sulfate ions on the surface.

[6] Movies may be downloaded from http://www.fz-juelich.de/isg/isg3/Giesen/ag-giesen1.htm#Movies.

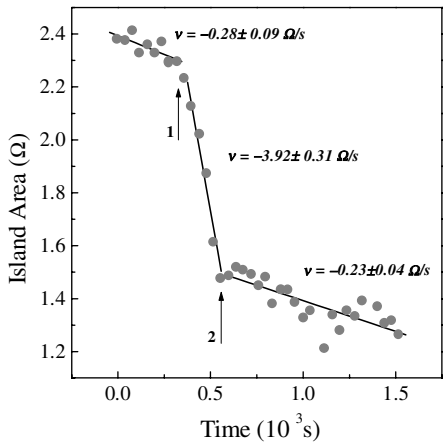

Figure 8. Rapid interlayer mass transport during Au island decay on Au(100) in 50 mM H_2SO_4 at −150 mV versus SCE. At arrow 1 a reconstruction line approaches the island which then undergoes a rapid decay. At arrow 2, the island eventually separates from the reconstruction line and the decay rate decreases. (Island area given in 10^3 Ω.)

For Cu(100), Cu(111) and Ag(111) in UHV e.g. one finds considerable larger step and kink energy values, $a_\parallel \gamma_{\mathrm{Cu}(100)} = 220$ meV [37], $a_\parallel \gamma_{\mathrm{Cu}(111)} = 270$ meV [37], $a_\parallel \gamma_{\mathrm{Ag}(111)} = 250$ meV [37], $\varepsilon_{\mathrm{Cu}(100)} = 128$ meV [61, 62], $\varepsilon_{\mathrm{Cu}(111)} = 117$ meV [37] and $\varepsilon_{\mathrm{Ag}(111)} = 97$ meV [37]. The values we find for γ and ε on Au(100) in 50 mM H_2SO_4 at +400 mV versus SCE are significantly smaller (59 and 51 meV, respectively), i.e. the step free energy and the kink energy are of comparable size. On Cu(111), Cu(100) and Ag(111) in UHV the kink energy is about a factor of two smaller than the step energy. EMT calculations by Stoltze [63] for the unreconstructed Au(100) surface in UHV, on the other hand, corroborate our findings for the Au(100) surface: Stoltze calculates 65 and 70 meV for the step and the kink energy, respectively. His values are somewhat larger compared to our studies in electrolyte but of comparable order of magnitude.

Concern may be raised in how far the values for γ and ε are influenced by specific assumptions used for the derivation of (3). The most critical assumption made in (3) is that the kink length is monatomic, i.e. $\varepsilon \gg k_B T$ or $\exp(-\varepsilon/k_B T) \ll 1$. In the case of Au(100), we have $\exp(-\varepsilon/k_B T) \sim 0.14$ which is a significant portion of 1. In order to estimate the influence of kinks of multiple atomic length on our result for the kink energy, one may use the ansatz that the energy of a kink of length $na_\perp$ is $n\varepsilon$. Then, one has for the step diffusivity

$$b^2 = \frac{a_\perp^2}{2\sinh^2(\varepsilon/2k_B T)}. \tag{14}$$

Using (14) in (3), one obtains

$$y\frac{\partial^2 y}{\partial x^2}k_B T \approx \frac{1}{2}\gamma a_\parallel \frac{1}{\sinh^2(\varepsilon/2k_B T)}. \tag{15}$$

With (10) and (12) we find

$$\sinh(\varepsilon/2k_B T) = 1.345 \pm 0.071 \tag{16}$$

which corresponds to

$$\varepsilon = 56 \pm 3 \text{ meV}. \tag{17}$$

This value for the kink energy is only slightly larger than the one determined under the assumption of monatomic long kinks as given in (13).

It is reasonable to assume that the step as well as the kink energy are potential dependent. Such potential dependent studies are currently performed in our group and will be published elsewhere [64].

At this point we want to discuss an issue of concern that may be raised when discussing STM results. In studies of atomic motion on surfaces, the problem arises in how far the results are influenced by the presence of the tunnelling tip. As has been demonstrated in [32], the tunnelling bias may locally induce electrochemical reactions such as metal dissolution. For potentials far from a phase transition it has been shown that moderate tunnelling parameters may prevent an influence of the tip on the analysis of atomic motion at the interface [32]. In the studies presented here we have not performed systematic measurements of the equilibrium island shape for different tunnelling parameters. This would have been an immense task considering that for each variation of the tunnelling parameters we would have to analyse several hundred islands to be able to compare statistically comparable data sets. We have therefore used a different procedure to check on a possible tip influence: if the island shape and the shape fluctuations would be influenced by the presence of the tip due to changes in atomic motion along the island perimeter one would expect that tip effects were more efficient for small islands since they contain relatively more periphery atoms. Hence, we checked for possible differences in the island equilibrium shape as a function of the island size and found no measurable deviations in the island shape. For one distinct potential around 350 mV we changed the tunnelling resistance from 0.23 to 0.19 GΩ and found no measurable difference in the equilibrium shape. In fact, even if there was a small influence of the tip and several atoms were shifted by several lattice spacings whenever the tip scans across an island edge, this influence would hardly be noticeable: most of the shape fluctuations, which are up to two orders of magnitude larger, occur during the time the tip scans across a totally different surface region. In particular, the latter argument holds also for the case of the island decay results discussed in the next paragraph. Hence, when averaging experimental results over a large number of individual (not too small) islands one may safely exclude a tip influence on the island data at least on Au(100) as studied here.

4.2. Island decay on Au(100) in 50 mM H_2SO_4

We have observed two different transport mechanisms during island decay as a function of the electrode potential. At +500 mV, the islands undergo normal Ostwald ripening via a diffusion limited decay mechanism. At −150 mV, the island decay is dominated by the re-formation of the (hex) surface reconstruction and the decay is detachment limited. The difference in the two decay mechanisms may be due to two reasons: first, at +500 mV the surface is covered by specifically adsorbed sulfate ions, whereas at −150 mV the surface is free of adsorbates. The presence of ions on the surface may considerably change the detachment barrier from kinks and the activation energy for terrace diffusion. As a consequence, the time-limiting step in the island decay may change. The energy balance between the detachment and the diffusion barrier may also sensitively depend on the surface: for Cu(111) [50] and Ag(111) [65] in UHV, e.g., the island decay is diffusion limited. On Cu(100) [66, 67] in UHV, however, the decay is detachment limited. Second, at +500 mV versus SCE, the island decay is dominated by *intra*layer mass transport whereas at −150 mV versus SCE, the shrinking of the islands is basically due to *inter*layer mass transport. Here, the time limiting step is most probably the incorporation of gold atoms into the Au(100) surface as

was also suggested by Magnussen *et al* [68] several years ago. If the incorporation is the time-limiting step, one may give an estimate for the terrace diffusion barrier: Skoluda and Kolb [69] measured the activation energy for the transition (hex) $\rightarrow$ (1×1) as a function of the electrode potential and found $E_{act} = 0.24$ eV at +480 mV and $E_{act} = 0.31$ eV at +530 mV. These values should be comparable with the activation energy for adatom incorporation during the $(1 \times 1) \rightarrow$ (hex) transition. That means that the detachment of atoms from an island edge and the diffusion on the terrace should have a lower activation barrier than 0.2–0.3 eV.

For the incorporation of gold atoms one may also consider a different mechanism which involves exchange of atoms at kinks in the island edge with the underlying terrace. Such a process was proposed by Magnussen *et al* [68] and Dakkouri [20] who qualitatively described the incorporation of atoms from islands into reconstruction lines when a line approaches the island edge. Dakkouri [20] indeed found that the re-formation of the reconstruction lines stops when no islands are left on the surface. In other words, the islands serve as nucleation centres for the potential-induced formation of the (hex) reconstruction. For atom exchange, no adatom detachment onto the terrace and no subsequent diffusion would be involved in the island decay process. The activation energy of such an exchange process could considerable differ from the data of Skoluda and Kolb. The existence of an exchange process as the pathway for the incorporation of gold adatoms into the surface is also confirmed by our observation of rapid island decay events when a reconstruction line makes contact with an island: we have compared the length change of a reconstruction line with the loss of atoms in the island and found that during rapid island decay all atoms detached from the island edge are directly incorporated into the reconstruction line which touched the island edge from below.

Further information on the activation barriers for the island decay are still lacking. Here, temperature-variable measurements are required to obtain, e.g. the sum of the adatom formation energy and the terrace diffusion barrier, $E_{ad} + E_{diff}$ ((6), (8)). Since in the equations for the diffusion limited decay (6) as well as for the detachment limited decay (8) the activation energy is given by $E_{ad} + E_{diff}$, one may be able to gain information about the influence of specifically adsorbed sulfate ions on the activation energies. For that purpose, however, also information on the potential dependence of the step free energy γ is necessary. The latter studies are currently performed in our group [64]. The temperature-variable experiments on the island decay are planned for the near future.

5. Summary

We have demonstrated that the analysis of equilibrium island shapes as developed for studies of homoepitaxial islands on metal surfaces in UHV may also be successfully applied to studies of islands on metal electrodes in contact with a liquid. Such investigations are the only available to date to gain information about step energies on metal electrodes in electrolyte. We have in particular studied Au islands on Au(100) in sulfuric acid close to the (hex)-(1×1) phase transition. We determine a step energy for steps along the atomically dense direction of 59 meV/atom and a kink energy of 51 meV.

From island decay studies at different electrode potentials we find that at high potentials where the surface is unreconstructed the decay of islands is diffusion limited. At low potentials where the reconstruction is re-established the island decay is detachment limited. Furthermore, rapid decay events are observed which is indicative of exchange processes between islands and the underlying terrace when a reconstruction line approaches an island edge.

Acknowledgments

We are indebted to U Linke for the preparation of the Au(100) electrodes. Fruitful discussions with H. Ibach and his critical reading of the manuscript are gratefully acknowledged. This work is partially supported by the Fonds der Chemischen Industrie, Germany.

References

[1] Dietterle M, Will T and Kolb D M 1995 *Surf. Sci.* **342** 29
[2] Batina N, Kolb D M and Nichols R J 1992 *Langmuir* **8** 2572
[3] Dietterle M, Will T and Kolb D M 1998 *Surf. Sci.* **396** 189
[4] Hölzle M H, Zwing V and Kolb D M 1995 *Electrochim. Acta* **40** 1237
[5] Kibler L A, Kleinert M and Kolb D M 1999 *J. Electroanal. Chem.* **467** 249
[6] Nichols R J, Beckmann W, Meyer H, Batina N and Kolb D M 1992 *J. Electroanal. Chem.* **330** 381
[7] Randler R, Dietterle M and Kolb D M 1999 *Z. Phys. Chem.* **208** 43
[8] Ziegler J C, Wielgosz R I and Kolb D M 1999 *Electrochim. Acta* **45** 827
[9] Shi Z, Wu S and Lipkowski J 1995 *Electrochim. Acta* **40** 9
[10] Xu J G and Wang X W 1998 *Surf. Sci.* **408** 317
[11] Moffat T P 1998 *J. Phys. Chem.* B **102** 10 020
[12] Schmidt U, Vinzelberg S and Staikov G 1996 *Surf. Sci.* **348** 261
[13] Staikov G and Lorenz W J 1999 *Z. Phys. Chem.* **208** 17
[14] Zei M S, Wu K, Eiswirth M and Ertl G 1999 *Electrochim. Acta* **45** 809
[15] Möller F, Magnussen O M and Behm R J 1995 *Electrochim. Acta* **40** 1259
[16] Hotlos J, Magnussen O M and Behm R J 1995 *Surf. Sci.* **335** 129
[17] Stickney J L, Villegas I and Ehlers C B 1989 *J. Am. Chem. Soc.* **111** 6473
[18] Cali G J, Berry G M, Bothwell M E and Soriaga M P 1991 *J. Electroanal. Chem.* **297** 523
[19] Goetting L B, Huang B M, Lister T E and Stickney J L 1995 *Electrochim. Acta* **40** 143
[20] Dakkouri A S 1997 *Solid State Ion.* **94** 99
[21] Vogt M R, Lachenwitzer A, Magnussen O M and Behm R J 1998 *Surf. Sci.* **399** 49
[22] Jeong H-C and Williams E D 1999 *Surf. Sci. Rep.* **34** 171
[23] Giesen M 2001 *Prog. Surf. Sci.* **68** 1
[24] Broekmann P, Wilms M, Kruft M, Stuhlmann C and Wandelt K 1999 *J. Electroanal. Chem.* **467** 307
[25] Ikemiya N, Nishide M and Hara S 1995 *Surf. Sci.* **340** L965
[26] Hirai N, Tanaka H and Hara S 1998 *Appl. Surf. Sci.* 130–2 506
[27] Hirai N, Watenabe K, Shiraki A and Hara S 2000 *J. Vac. Sci. Technol.* B **18** 7
[28] Kolb D M, Ullmann R and Ziegler J C 1998 *Electrochim. Acta* **43** 2751
[29] He Y and Borguet E 2001 *J. Phys. Chem.* B **105** 3981
[30] Hirai N, Watanabe K and Hara S 2001 *Surf. Sci.* **493** 568
[31] Giesen M, Dietterle M, Stapel D, Ibach H and Kolb D M 1997 *Surf. Sci.* **384** 168
[32] Giesen M, Randler R, Baier S, Ibach H and Kolb D M 1999 *Electrochim. Acta* **45** 533
[33] Giesen M and Kolb D M 2000 *Surf. Sci.* **468** 149
[34] Baier S and Giesen M 2000 *Phys. Chem. Chem. Phys.* **2** 3675
[35] Giesen M and Baier S 2001 *J. Phys.: Condens. Matter* **13** 5009
[36] Baier S, Dieluweit S and Giesen M 2001 *Surf. Sci.* at press
[37] Giesen M, Steimer C and Ibach H 2001 *Surf. Sci.* **471** 80
[38] Khare S V and Einstein T L 1996 *Phys. Rev.* B **54** 11 752
[39] Schlößer D C, Verheij L K, Rosenfeld G and Comsa G 1999 *Phys. Rev. Lett.* **82** 3843
[40] Steimer C, Giesen M, Verheij L and Ibach H 2001 *Phys. Rev.* B **64** 085416
[41] Dakkouri A S, Randler R and Kolb D M 1997 *Proc. Symp. on The Electrochemical Double Layer* ed C Korzeniewski and B E Conway (Pennington, NJ: The Electrochemical Society)
[42] Xia X H, Schuster R, Kirchner V and Ertl G 1999 *J. Electroanal. Chem.* **461** 102
[43] Dakkouri A 1996 *PhD Thesis* University of Ulm, Germany
[44] Kolb D M 1996 *Prog. Surf. Sci.* **51** 109
[45] Bartelt N C, Einstein T L and Williams E D 1990 *Surf. Sci.* **240** L591
[46] Lifshitz L M and Slyozov V V 1961 *J. Phys. Chem. Solids* **19** 35
[47] Wagner C 1961 *Z. Elektrochem.* **65** 581
[48] Chakraverty B K 1967 *J. Phys. Chem. Solids* **28** 2401

[49] Wynblatt P and Gjostein N A 1975 *Progress in Solid State Chemistry* ed J O McCaldin and G Somorjai (Oxford: Pergamon) p 21
[50] Icking-Konert G S, Giesen M and Ibach H 1998 *Surf. Sci.* **398** 37
[51] Kolb D M and Schneider J 1986 *Electrochim. Acta* **31** 929
[52] Kolb D M and Schneider J 1985 *Surf. Sci.* **162** 764
[53] Zei M S, Lehmpfuhl G and Kolb D M 1989 *Surf. Sci.* **221** 23
[54] Besocke K, Krahl-Urban B and Wagner H 1977 *Surf. Sci.* **68** 39
[55] Gao X, Edens G J, Hamelin A and Weaver M J 1994 *Surf. Sci.* 318 1
[56] Theis W, Bartelt N C and Tromp R M 1995 *Phys. Rev. Lett.* **75** 3328
[57] Rosenfeld G, Morgenstern K, Esser M and Comsa G 1999 *Appl. Phys.* A **69** 489
[58] Giesen M, Icking-Konert G S and Ibach H 1998 *Phys. Rev. Lett.* **80** 552
[59] Giesen M, Icking-Konert G S and Ibach H 1999 *Phys. Rev. Lett.* **82** 3101
[60] Giesen M and Ibach H 2000 *Surf. Sci.* **464** L697
[61] Giesen-Seibert M, Jentjens R, Poensgen M and Ibach H 1993 *Phys. Rev. Lett.* **71** 3521
[62] Giesen-Seibert M and Ibach H 1994 *Surf. Sci.* **316** 205
[63] Stoltze P 1994 *J. Phys.: Condens. Matter* **6** 9495
[64] Dieluweit S, Ibach H and Giesen M 2002 *Faraday Discuss. Chem. Soc.* at press
[65] Morgenstern K, Rosenfeld G and Comsa G 1996 *Phys. Rev. Lett.* **76** 2113
[66] Hannon J B, Klünker C, Giesen M, Ibach H, Bartelt N C and Hamilton J C 1997 *Phys. Rev. Lett.* **79** 2506–09
[67] Klünker C, Hannon J B, Giesen M, Ibach H, Boisvert G and Lewis L J 1998 *Phys. Rev.* B **58** R7556
[68] Magnussen O M, Hotlos J, Behm R J, Batina N and Kolb D M 1993 *Surf. Sci.* **296** 310
[69] Skoluda P and Kolb D M 1992 *Surf. Sci.* **260** 229–34